
Understanding the low cycle fatigue of additive manufactured Inconel 718: a crystal plasticity modelling approach

Wenye Ye

Department of Chemical and Materials Engineering,
University of Nevada,
1644 N. Virginia Street, Reno,
NV, 87557, USA
Email: wenye.ye@nevada.unr.edu

Pankaj Kumar*

Department of Mechanical Engineering,
University of New Mexico,
1, MSC01 1150, Albuquerque,
NM 87131, New Mexico, USA
Email: pankaj@unm.edu
*Corresponding author

Leslie T. Mushongera

Department of Chemical and Materials Engineering,
University of Nevada,
1644 N. Virginia Street, Reno,
NV, 87557, USA
Email: lmushongera@unr.edu

Abstract: Additive manufacturing provides an opportunity to manufacture complex geometry components of Inconel 718 efficiently. However, it is essential to develop an understanding of microstructure dependent fatigue to ensure the safety of these components in applications. The various microstructure constituents affect the fatigue performance. Among various microstructure constituents, the grain morphology is known to significantly affect fatigue performance. In the present study, a rigorous analysis of the microstructure effect considering the typical columnar (as-built) and equiaxed (annealed) grain on the fatigue behaviour has been studied using crystal plasticity modelling. The analysis indicated that at low cycles, the fatigue performance of columnar microstructure is better than the equiaxed microstructure. On the other hand, the equiaxed microstructure at higher cycles shows higher fatigue performance than the columnar morphology. Stress relaxation due to local plastic deformation in both the columnar and equiaxed grain microstructure plays a role in delaying crack initiation during cyclic loading.

Keywords: Inconel 718; additive manufacturing; fatigue; cyclic stress-strain loops; crystal plasticity.

Reference to this paper should be made as follows: Ye, W., Kumar, P. and Mushongera, L.T. (2021) ‘Understanding the low cycle fatigue of additive manufactured Inconel 718: a crystal plasticity modelling approach’, *Int. J. Theoretical and Applied Multiscale Mechanics*, Vol. 3, No. 4, pp.313–328.

Biographical notes: Wenye Ye is a PhD candidate in the Department of Chemical and Materials Engineering at the University of Nevada, Reno. He completed his Bachelor’s degree from the Chongqing University, Chongqing, China, and Master’s from the Ruhr-Universität Bochum, Bochum, NW, Germany. His PhD research focus is on multi-scale modelling of deformation behaviour in polycrystalline materials. His specific research interests are crystal plasticity and molecular dynamics simulation.

Pankaj Kumar is an Assistant Professor in the Department of Mechanical Engineering at the University of New Mexico. His research focuses on the experimental and computational approach to elucidate the processing-microstructure-mechanical property relationship in metallic systems. His core research areas are advanced manufacturing and microstructure, and materials design.

Leslie T. Mushongera is an Assistant Professor of Materials Science and Engineering at the University of Nevada Reno. His expertise lies in developing physics-based computational modelling and design tools that enable the study of various physical phenomena in structural materials at different length scales to determine structure-property relations. His research group focuses on addressing fundamental research aspects and concurrent implementation of this knowledge into high fidelity computational models.

This paper is a revised and expanded version of a paper entitled ‘Fatigue life prediction of additive manufactured IN718 superalloys’ presented at TMS Annual Meeting & Exhibition, San Diego, USA, 23–27 February 2020.

1 Introduction

Additive manufacturing (AM) techniques have provided new opportunities for fabricating near-net-shape metallic components with complex geometries, which was difficult to achieve in traditional manufacturing techniques. These techniques enable manufacturing complex mechanical parts in near net shape and even fabricating whole mechanical assembly in about ready-to-use conditions. AM ensures a unique approach to manufacturing, product development, and supply chain. The product can be developed as a whole in AM rather than in parts like traditional manufacturing, leading to raw material saving, energy-saving, and reduced environmental impact, therefore increasing over cost-efficiency. Hence, AM attracts significant attention of the manufacturing industries targeting the fabrication of highly customised parts for high-end engineering applications, such as aviation, biomedical, and aerospace.

Different types of AM techniques have been developed over the last few years and are classified based on the feedstock form such as powder or wire, energy sources, e.g., laser or electron beam, and powder feeding techniques, e.g., as powder bed or blown powder. Due to unique solidification during AM, the microstructure evolution is very

distinct regarding the microstructure observed in the conventional route. High residual stresses, textures, and defects such as porosity due to voids, pinholes, and unmelted powder particles, are the microstructural characteristics of AM alloy. These characteristics have a significant impact on mechanical properties (Frazier, 2014; Lewandowski and Seifi, 2016). Many studies focusing on improving the residual stress, porosity, and texture characteristics to enhance the mechanical performance can be found in the literature. Ranging from optimising the scanning strategy both in the laser and electron-based AM to post-processing has been evaluated, and success in controlling the microstructure, thereby, improved mechanical properties have been shown. The columnar and cellular sub-structure grains in the built-direction with the equiaxed grains are typical microstructures of an AM manufactured alloy in terms of grain shape. The grain sizes, however, varies depending on the AM process and the respective process parameters. The fine equiaxed grains are desirable for a good tensile and fatigue performance of a metallic system. On this basis, attempts have been made to optimise the AM processing parameters and scan strategy to achieve the equiaxed grains. The goal has been to break the columnar grains extending up to mm length and transform the grains toward the equiaxed grains. Early studies demonstrated that a controlled microstructure could be achieved in the electron beam AM by hopping the energy beam (Biffi et al., 2020; Dehoff et al., 2015). Similar, impact on the microstructure has been and observed in laser-based AM (Shi et al., 2020). Using a pulsed laser scan than the continuous beam help to modify the microstructure in more equiaxed grains. This grain modification in the modified beam scan strategy has been attributed to the thermal front change. This implies that the transition between the columnar and equiaxed grain is controlled by the solidification rate and the spatial-temporal variation of the thermal gradients. In general, the grain structure has a significant impact on the mechanical properties of metallic materials. Kumar and Chandran (2017), in a study, demonstrated the effect of the typical grain structure on the tensile properties of Ti-6Al-4V alloy when the porosity level exceeds 99%. Their studies demonstrate that the fully lamellar structure shows a wide variation in strength and ductility. The smaller the interlamellar spacing higher the tensile strength and vice-versa. The equiaxed grains with finer grain sizes and smaller α exceeds the strength of the columnar grains. The fatigue performance of the Ti-6Al-4V alloy was shown to be more sensitive to the columnar grains when the porosity exceeds 99% – larger the columnar colonies, poor the fatigue performance (Cao and Ravi Chandran, 2016). Also, it has been observed that the equiaxed grain has better fatigue resistance than the columnar grain microstructure. This has been attributed to high crack growth resistance in the equiaxed microstructure. The AM processes yield high-density (>99.9%) materials with very few pores randomly distributed in the microstructure. In this case, therefore, the grain shape and size become a predominant factor in deciding the mechanical performance of the materials. Many reviews have been published on the tensile properties of AM materials. These reviews indicates the tensile properties of AM materials varies over a wide range compared to its conventionation parts. Bajaj et al. (2020), in their review on AM steels, showed that the tensile strength of the austenitic SS (stainless steel) varies in a range of 480–800 MPa while the conventionally produced SS varies in 580–590 MPa (Lewandowski and Seifi, 2016). The superior strength and a large variation of AM SS are attributed to the formation of hierarchical microstructures consisting of columner grains, and fine cellular grains. Although the tensile properties on AM processed material are well studied and achieved the performance closed to the conventional material, the microstructure and properties relationships are still not well understood making AM

untrustable to use in real applications. Filling the gap in understanding of microstructural influence on the properties are essential for predicting the performance of AM materials in structural applications.

A major concern of AM metallic systems is their fatigue performance. Fatigue failure is a common failure method of the structural components – the fatigue phenomena triggered by the local microstructural characteristics. The general conclusion is that the as-AM components show the lowest fatigue strength compared to the wrought counterparts. The geometric defects such as porosity, surface roughness, and texture significantly influence the fatigue performance of AM materials. Inconel 718 (IN 718) is a critical alloy for aviation and aerospace applications, where high fatigue resistance is vital. Several studies focusing on evaluating the fatigue performance of IN 718 manufactured by different AM techniques have been published in the literature. Due to large differences in processing parameters and feed stock materials, and variations in post-AM, etc. it is difficult to evaluate the comparative fatigue strength of AM IN 718 and estimate the effect of different microstructural aspects on fatigue performance. General observation suggests that the pore sizes in AM materials significantly impact the fatigue strength. It is also indicated that the pore locations in the loading cross-section significantly alter the fatigue strength (Balachandramurthi et al., 2018; Cao et al., 2015). This implies that due to a larger variation in pore characteristics, a large scatter in fatigue strength has been observed. Eliminating the characteristic pores will help to reduce the scatter in fatigue data, and enhance the fatigue resistance of AM IN 718. With the aim of reducing the porosity, many studies used a post-AM hot isostatic press (HIP) for the as-built materials. Many of these studies indicated an increase in fatigue strength, which has been attributed to the reduction in porosity in the microstructure. Some studies, however, showed a reduction in fatigue strength after HIPing. The reduction in fatigue strength has been attributed to the microstructural effects. The fatigue strength is related to the local crack initiation during the fatigue cycles. Cao et al. (2015) suggested that crack initiation is a competitive mechanism and which microstructural characteristics dominate the crack initiations depend on their size. If the pores are larger than the characteristic grains, the pore will dictate the fatigue performance of a material and vice-versa. Both the defects and the microstructural characteristics affect the fatigue performance depending on the competitive mechanism between them. Many studies focusing on identifying the effects of pores on fatigue behaviour have been performed. Although an initial understanding of the pore effect on the fatigue behaviour has been developed, more studies filling the various microstructure gaps are needed to establish the effect of the defects on AM IN 718. It is also well known that the grain characteristics have a significant impact on fatigue performance. According to a NASA (2017) report, the final microstructure of a metal AM part must consist of a "...predominantly uniform and non-directional grain structure, free of remnants of the as-built structure" for the aerospace application. This illustrates the significance of identifying the impact of the grain structure on fatigue performance. However, very few attempts have been made to understand the relationship between grain structure and the fatigue strength of AM IN 718.

In the present study, using the crystal plasticity (CP) approach, the effect of the specific columnar and equiaxed grains on the fatigue performance of AM IN 718 material will be evaluated. This specific study did not consider the defects in the microstructure. While this study purely focuses on the effect of the specific grain morphologies, it will

establish both upper and lower bound for the fatigue strength of AM IN 718 as dictated by the microstructure.

2 Methods

The microstructures of IN 718 obtained from laser powder bed fusion (L-PBF) AM technique has been considered in this study. The as-built IN 718 with porosity <1% is considered as the typical equivalent of the columnar microstructure of AM IN 718. The detailed manufacturing process can be found elsewhere (Kumar et al., 2019). A post-AM heat-treated IN 718 with equiaxed microstructure has been considered as the equiaxed equivalent grain morphology to study in this work. The grain morphologies were obtained on both as-built and heat-treated IN 718 samples using electron backscattered diffraction (EBSD) with a step size of 0.3 microns. The grain morphologies obtained from the 2D EBSD map were used to reconstruct a 3D grain morphology using a theoretical model as described below. The 2D EBSD maps provided statistics on the necessary microstructural constitutions such as the grain size, morphology, the spatial orientation of the crystal structure in the form of the three Euler angles, and the distribution of twins for reconstruction. The 3D reconstructed representative microstructures (RMs) were used as input for the CP modelling to analyse the fatigue performance. In this study, the volume fraction is considered same for all cases in the CP modelling.

2.1 Reconstruction of 3D microstructure

The conversion of 2D data to the 3D RMs with equiaxed grains was performed in a multi-step iterative process. The following assumptions were made; the 2D grain size scales by $4/\pi$, and the 3D grain size follow a lognormal distribution. This assumption is made based on microstructural considerations. The base 3D microstructure was constructed by the statistics retrieved from EBSD using the StatsGenerator tool in DREAM3D. The grains in the base microstructure for equiaxed grains were reconstructed with a size slightly bigger than that measured from EBSD in order to account for the twins. It was necessary to limit the number of grains and the size of the RMs, by adjusting the grain size distribution for the computational consideration. Considering the large fraction of twins observed in the microstructure in the heat-treated IN 718, it is important to account for these features in the CP. Since the filtering of EBSD data in Dream3D resulted in the elimination of some important microstructural features (e.g., twins), an insertion code was used to systematically re-insert these microstructural features in the as generated RMs. Twin fractions with volume fractions corresponding to EBSD statistics were inserted along with one of the randomly chosen $\{111\}$ planes in randomly chosen grains of the parent microstructure for the representative 3D microstructures with equiaxed grains of heat-treated samples. The process was iterated until the experimental microstructural attributes and virtual microstructures were similar. The similarity was evaluated on the basis of the mean of the grain size distribution, the twin fraction, and the Taylor factor, which accounts for the averaging of the grain orientations overall grains. For the reconstruction of columnar morphology in as-built IN 718, the grains were designed with a proportion of 10:2:1 for length, width, and depth, respectively. Then, defining the axis Euler angle, i.e., the inclination angle for grains as

three categories, 45°, 135°, and 90° along y -direction of the representative 3D microstructures. The meshing of both microstructure morphologies was done using Gmsh considering four-node tetrahedral elements (C3D4).

2.2 The CP modelling framework

The CP offers a framework of plasticity that uses both the slip rate and evolution of the microstructural variables. In this work, the CP finite element (CPFE) model developed based on deformation of the polycrystalline aggregates at large scale. To investigate the deformation of IN 718, a FCC unit structure with 12 active slip systems were considered. The previous study indicates that all 12 slip systems in IN 718 can be active during the plastic deformation [Cruzado et al., (2017), p.718]. In this approach, total deformation gradient F can be given as elastic part (F^e) and plastic part (F^p) as (Lee, 1969):

$$F = F^e F^p. \quad (1)$$

The plastic contribution F^p in equation (1) is related to irreversible (plastic) permanent deformation beyond the yield point. The plastic velocity gradient L^p is determined in terms of to slip rate $\dot{\gamma}_\alpha$ of the active slip system α and the Schmidt factor that consists of slip direction vector s_α and the vector normal to the slip plane m_α , respectively, written as:

$$L^p = \sum_{\alpha=1}^N \dot{\gamma}_\alpha (s_\alpha \otimes m_\alpha) \quad (2)$$

where N is the number of (active) slip systems. The plastic deformation can be written in a relation with the plastic strain rate:

$$\dot{p} = \sqrt{\frac{2}{3} L^p : L^p} \quad (3)$$

All the slip systems were assumed to be active during the strain hardening process, and the shearing rates with respect to their resolved shear stress is given by the following power law power-law flow rule (McGinty, 2002).

$$\dot{\gamma}_\alpha = \dot{\gamma}_0 \left| \frac{\tau^\alpha - \chi^\alpha}{g^\alpha} \right|^{1/m} \text{sgn}(\tau^\alpha - \chi^\alpha) \quad (4)$$

where $\dot{\gamma}_0$ is the reference shear strain rate, τ^α , χ^α , and g^α are resolved shear stress, back stress, threshold resistance to dislocation motion, and the drag stress on the α^{th} slip system, respectively. m is the strain rate-sensitivity exponent. The drag stress evolves following Armstrong and Frederick's (1966) relation

$$\dot{g}_\alpha = H \sum_{\beta=1}^N a^{\alpha\beta} |\dot{\gamma}_\beta| - R g_\alpha \sum_{\beta=1}^N |\dot{\gamma}_\beta| \quad (5)$$

where the parameters H and R are the direct hardenings and dynamic recovery coefficients, respectively. The term $a^{\alpha\beta}$ is the latent hardening of the matrix (Jackson and Basinski, 2011; Kocks and Brown, 1966; Wu et al., 2018). The diagonal terms for the self

hardening assumed to be 1 while the cross section-terms for the latent hardening considered to be 1.2. The back stress evolved as per the following equation.

$$\dot{\chi}^{(\alpha)} = A_{dir}\dot{\gamma}^{(\alpha)} - A_{dyn}\chi^{(\alpha)}|\dot{\gamma}^{(\alpha)}| \quad (6)$$

The parameters A_{dir} and A_{dyn} are the direct hardening and dynamic recovery coefficients, respectively.

3 Results and discussion

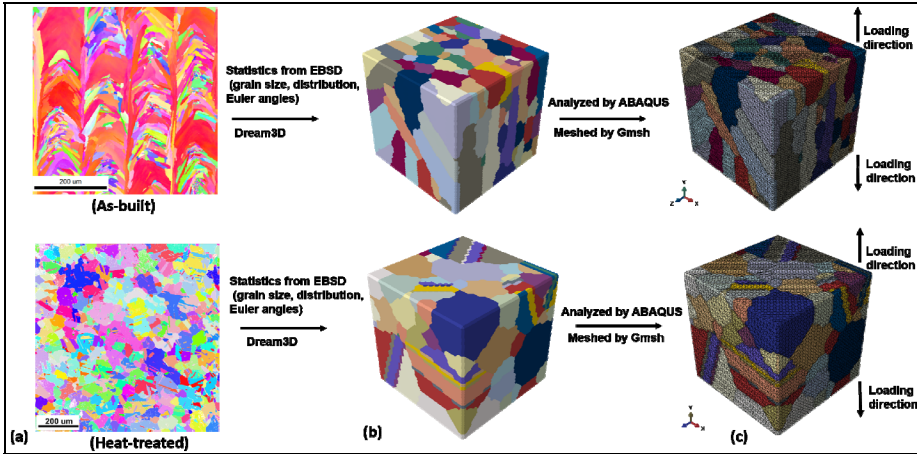
3.1 Grain morphology of as-built and heat-treated AM IN 718

The microstructural morphologies of the as-built and heat-treated L-PBF samples was examined on the transverse planes parallel to the build direction. The RM of as-built and heat-treated samples is shown in Figure 1(a). The microstructure of as-built consists of large and interconnected columnar grains along with random columnar grains, as shown in Figure 1(a). This demonstrates the formation of the characteristic solidification microstructure of IN 718. In general, the excess energy re-melts the already solidified layer and develops a large interconnected columnar grain in the direction of laser scanning. This as-built microstructure observation can be corroborated with the literature data (Aydinöz et al., 2016). Although the columnar grain sizes varied depending on the laser processing parameters in the literature, a similar morphology has been seen for the as-built IN 718. This demonstrates the columnar grains are the typical grain morphology observed for IN 718 when manufactured using laser-based AM techniques. On the other hand, the heat-treated sample indicates an equiaxed grain morphology in the microstructure along with the annealing twins. The formation of annealing twins after heat treatment in AM IN 718 is well known. The annealing twins have also been observed in hot isostatic pressed (HIPed) AM IN 718 (Babamiri et al., 2020). This demonstrates the twin is an important microstructure feature that can impact the mechanical performance of AM IN 718. The generated 3D RM [Figure 1(b)] with the cube edge of 210 μm represent statistical equivalency in terms of microstructural attributes. The meshed microstructure as considered for CP calculation is shown in Figure 1(c). The direction indicates the loading condition in CP simulation to account for microstructural characteristics on the fatigue performance.

For computational reasons, we generated a set of five RMs consists of 124–197 grains and an edge of 210 μm , as shown in Figure 2, instead of analysing a large EBSD microstructure. Each RMs is named 1 to 5 for columnar and equiaxed grain morphologies. The obtained RMs were characterised by columnar and equiaxed grains consistent with the morphologies observed in as-built and as-heat treated AM IN 718 respectively. These RMs were used as the microstructural basis for the CP simulations to capture the fatigue variation. These grains are large enough to capture the macro stress-strain curve and fatigue analysis. In the heat-treated samples, the twin fraction as high as 50% fraction was observed in the present study as shown in Figure 2. The twin fraction as high as 65% has also been reported in the heat treated AM IN 718 (Li et al., 2019). The formation of twins during annealing of AM 718 is facilitated by the residual stress in the materials. Thus, depending on the laser processing parameters and the heat treatment cycles, the number fraction of twin boundaries will change. In general, the

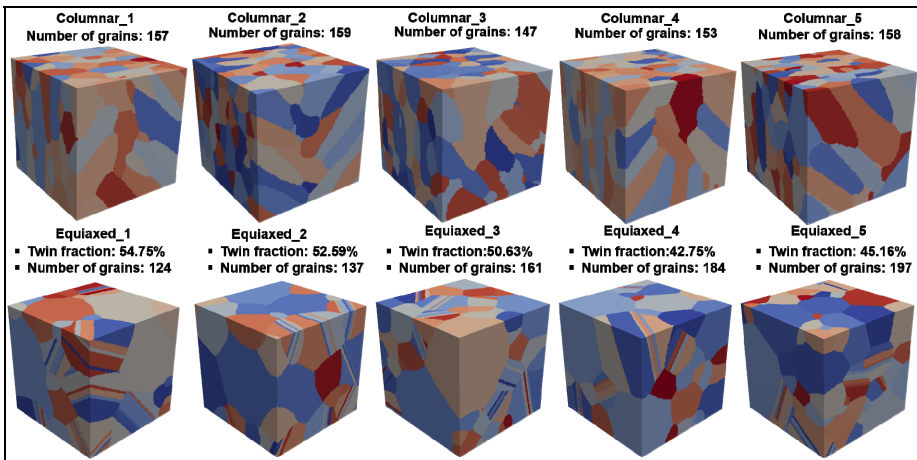
higher fraction of special boundary enhances the mechanical performance of the material (Holland et al., 2018; Ni et al., 2019; Vikram et al., 2020). The meshed RMs, which was done using Gmsh in ABAQUS, were used in the CP modelling code to calculate the cyclic stress-stain behaviour and the fatigue performance.

Figure 1 (a) Columnar and equiaxed microstructures that are observed from experimental EBSD data for as built and heat-treated samples (b) A representative microstructure with columnar and equiaxed grains based on the statistics and grain morphology from 2D EBSD map (c) Meshed microstructures with tetrahedral elements (see online version for colours)



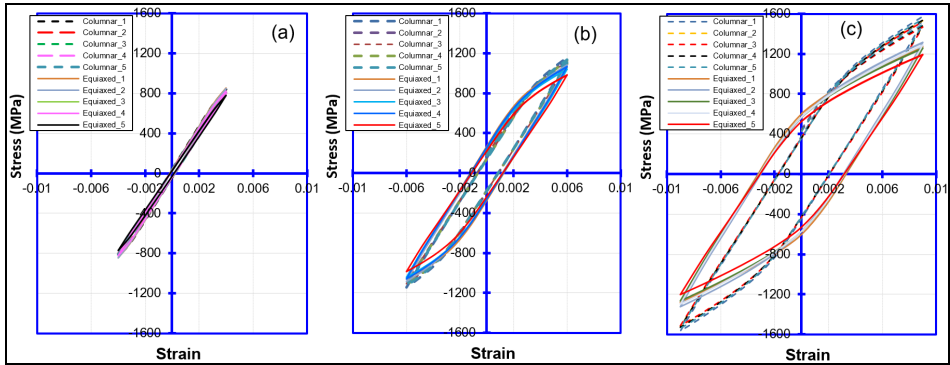
Notes: The loading directions applied to both representative microstructures is along the y-axis during simulation. The edge of the cube corresponding to columnar and equiaxed microstructure are 90 μm and 210 μm , respectively.

Figure 2 The set of five representative 3D microstructures for columnar (upper set) and equiaxed (lower set) grains used in the simulations (see online version for colours)



Notes: The edge of the cube corresponding to columnar and equiaxed microstructure are 90 μm and 210 μm respectively.

Figure 3 Stress-strain loops after three cycles in CP modelling at $\Delta\varepsilon$ of, (a) 0.8% (b) 1.2% (c) 1.8% (see online version for colours)



Notes: Both microstructure shows elastic deformation at lower strain amplitude and with increasing $\Delta\varepsilon$, plastic deformation dominates and cyclic hardening observed. The columnar microstructure shows higher hardening as compared to the equiaxed microstructure.

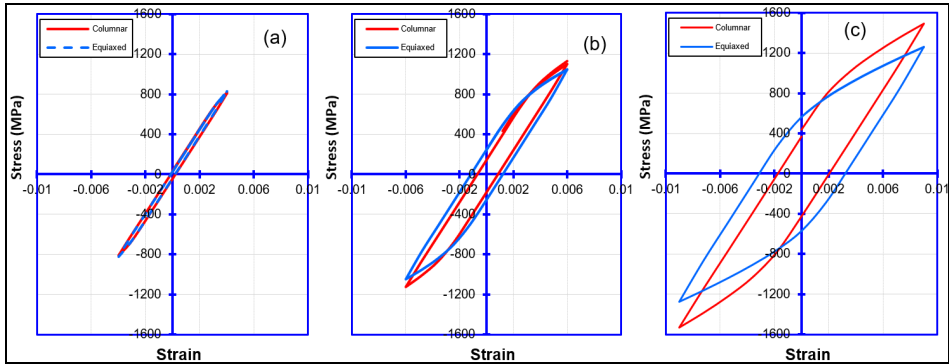
3.2 Cyclic stress response behaviour

The stress-strain loop at the strain amplitudes ($\Delta\varepsilon$) 0.8%, 1.2%, and 1.8% for each of the RMs (Figure 2) after three cycles in CP modelling at room temperature is presented in Figures 3(a)–3(c). The loading orientation to generate the stress-strain loops is shown in Figure 1(c). At the strain amplitude of 0.8%, each RMs (both columnar and equiaxed) exhibit predominantly elastic deformation with peak stress of 800 MPa during the cyclic loading. As the strain amplitude increased to 1.2%, the loops width or area increased, indicating the plastic deformation during cyclic loading. In all cases, the increase in peak stresses can be seen. The increase in the stress indicates the cyclic hardening of the microstructure during the cyclic loading. With further increase in strain amplitude to 1.8%, the width (or area) of the loop increased, showing the dominance of the plastic deformation during cyclic loading at this strain amplitude. The change in the loop shape with increased strain amplitude indicates that more strain energy is dissipated in each cycle, thereby reducing the fatigue life after each cycle. The peak stresses for columnar RMs vary between 1,467–1,522 MPa, while the equiaxed RMs have shown a peak stress variation between 1,191–1,289 MPa. The variation in the peak stress of columnar grains may be attributed to the grain orientation or texture of each RMs (Zhou et al., 2018). It is known that the columnar grains are highly anisotropic, and the stress distribution during loading will depend on the grain orientation with respect to the loading direction. The difference in hardening behaviour of each equiaxed RMs can be attributed to the difference in twin fraction and the number of grains. The twins have been considered as the barrier for dislocation movement. Increasing the dislocation storage near the twin region leads to a reduction of the free length for dislocation motion. The number of grains determine the size of grains in the given volume fraction of microstructure. As the number of grains increases the grain size decreases, thus limiting the free length of dislocation motion within the grains. It can also be noted that the peak stress increased with an increase in strain amplitude irrespective of the grain morphologies. This behaviour indicates that material cyclic hardened with increasing strain amplitude in the

range of 0.8% and 1.8% at room temperature. This can be correlated with increasing the dislocation activities with the cyclic deformation.

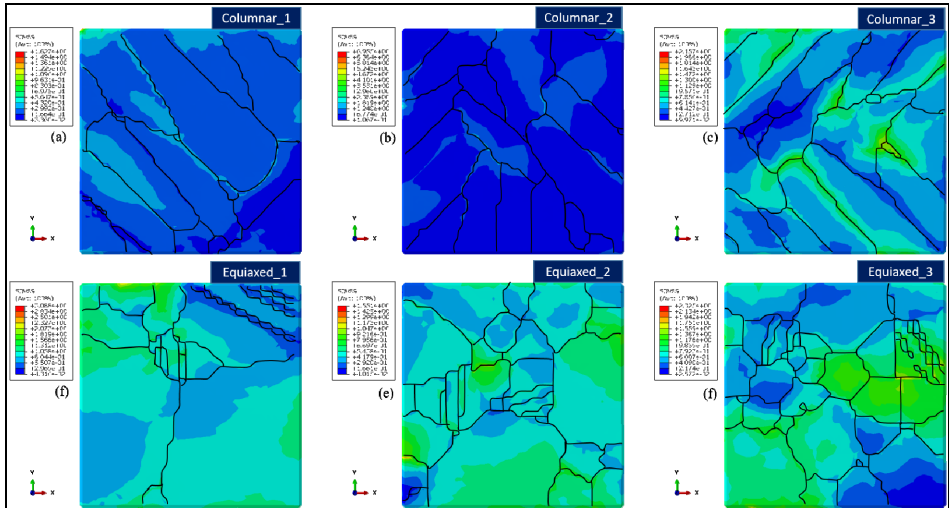
The average stress-strain loops of the columnar and equiaxed SEMs after three cycles are presented in Figures 4(a)–4(c). Although the peak stress is increased, the loop’s height gradually decreased with an increase in the strain amplitude for the equiaxed microstructure compared with the columnar microstructure.

Figure 4 Stress-strain loops after three cycles for average RMs at $\Delta\epsilon$ of, (a) 0.8% (b) 1.2% (c) 1.8% (see online version for colours)



Notes: Both loops indicated cyclic hardening, the peak stresses are higher for columnar compared to equiaxed microstructure at the strain amplitude increased.

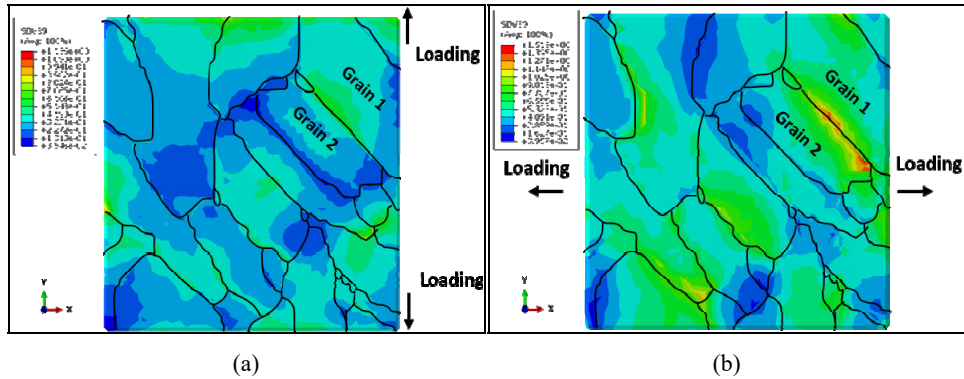
Figure 5 (a) (b) (c) Energy stored during the deformation in three set of RMs with columnar microstructure (d) (e) (f) Three set of equiaxed microstructure (see online version for colours)



Notes: The stored energy during deformation (upper set) and equiaxed (lower set) grains used in the simulations. The edge of the square corresponding to columnar and equiaxed microstructure are 90 μm and 210 μm respectively.

This demonstrates the hardening behaviour of both the microstructure is very different. This behaviour is clearly visible at higher strain amplitude. It seems the rate of hardening in the columnar grains is higher compared to the equiaxed grains with deformation. This behaviour can be correlated with the difference in dislocation densities between the two microstructures.

Figure 6 Energy stored during the deformation in columnar microstructure when the loading direction, (a) vertical (b) horizontal (see online version for colours)



Note: The edge of the square is 90 μm .

To understand the difference in deformation behaviour, the stored energy (SE) maps for each columnar and equiaxed microstructure were generated at an $\Delta\epsilon$ of 1.8%. The SE maps of both the columnar and equiaxed microstructure are given in Figure 5. The map generated using CP simulation in three sets of each columnar and equiaxed are presented in Figures 5(a)–5(c) and Figures 5(d)–5(f), respectively. The numbers of the microstructure correspond to initial SEMs that developed using the experimental data. The SE map indicates that depending on the microstructure characteristics, deformation energy can be stored homogeneously or non-homogeneously. The energy in columnar microstructure specifically stored at the grain boundaries (GBs), as seen in Figures 5(a)–5(c). This demonstrates that during cyclic loading, stresses and the corresponding strains concentrate at these locations. Dislocations accumulate within the GBs with increasing deformation as this act as a strong barrier for the dislocation glide and provide the strain localisation sites. With increasing strain, the concentration of dislocations increased at the GBs. As the deformation continues, more stress is required to overcome the backstress produced by dislocation interactions for a dislocation to glide at the GBs, leading to hardening in the grains. When the stress reaches the fracture stress, the crack initiates from this localised microstructure. In the case of the equiaxed grains, when the stress at the GBs increased significantly, the new deformation mechanism operates, leading to a reduction in hardening. Initially, a similar dislocation density may form due to deformation in the two microstructures. With increasing strains, the gradually-accumulated dislocation within the microstructure activates the slip bands and promotes the dislocation annihilation process in the equiaxed microstructure (Zhao and Chen, 2020). However, due to the boundary characteristics of the columnar grains, the crack initiates without any dislocation annihilation. Due to this, the orientation of columnar grains becomes important. The grain orientation with respect to the loading direction dictates the dislocation initiation and glide, as can be seen from Figure 6. The

microstructure map indicates that near the loading surface, the SE is comparatively higher than the other location of the microstructure. To understand the orientation effect within the grain, we considered grains 1 and grain 2. As shown in Figures 6(a) and 6(b), the boundary between grain 1 and grain 2, the magnitude of SE, are different. In horizontal loading, energy stored at the specific GB is an order higher than when loaded vertically. This indicates the location of fatigue crack initiations, and thereby the fatigue response will be different when the grain orientation to the loading direction changes. This demonstrates that the deformation in columnar microstructure largely depends on its orientation or texture during loading cycles. This study indicates that the fatigue cracks initiate from the columnar boundaries during the loading cycles. The crack initiation from the columnar GBs has been shown earlier experimentally in various materials.

3.3 *S-N behaviour*

The predicted S-N curves for the two microstructures are shown in Figure 7. To predict the S-N curve from the CP simulation, a SE criterion is adopted (Ye et al., 2020). The following steps were followed:

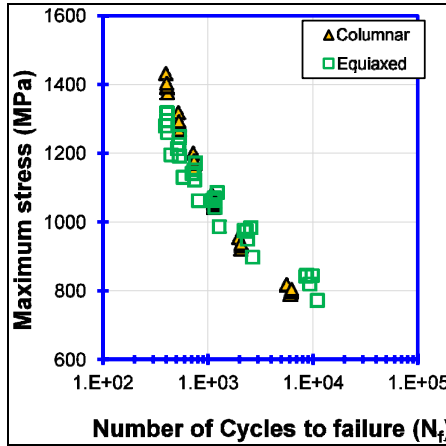
- 1 Integrate area under experimental hysteresis loop and use accumulated energy at specimen failure as our crack nucleation criteria.
- 2 Calculate accumulated energy from CP model.
- 3 Once the model saturates, the energy was extrapolated with increasing number of cycles.
- 4 Calculate number of cycles until failure.

The uniqueness of this approach is it inherently accounts for the localisation of slip and the dislocation densities which in part influence strain localisation and the locally SE. We used the experimental data (Deng et al., 2019) to calibrate the CP model. Energy per cycle per unit volume associated with the plastic deformation calculated from the experimental stress-strain hysteresis loop using the equation $\dot{U}^{\text{exp}} = \int |\sigma : d\epsilon^p|$. Based on this, the critical SE for crack initiation, G_c was calculated from the experimental data as:

$$G_c = \int_1^{ss} \dot{U}^{\text{exp}} \Delta V dN + \int_{ss}^{N_f} \dot{U}^{\text{exp}} \Delta V dN \quad (7)$$

$\int_{ss}^{N_f} \dot{U}^{\text{exp}} \Delta V dN$ term of equation (7) is the SE, ΔV is a length scale normalised characteristic storage volume defined by the dislocation density. It records SE from the first cycle to the cycle of saturated loop (*ss*), until the number of cycles of failure (N_f). ΔV does not change when the material achieves the steady state. In steady state the dislocation density also becomes stable. The number of cycles to achieve steady state is comparatively small compared with number of cycles that initiate cracks. Hence, the value of ΔV is set as 1 in this study. The unique critical SE value is expected to be independent of the loading conditions. Obtaining a single critical SE is challenging due to the reservations in experimental measurements. Hence, we adopt the averaged value G_c obtained at different applied strain amplitudes for fatigue crack initiation.

Figure 7 S-N curve of two microstructure at a stress ratio (R_σ) of -1 predicted using the CP model (see online version for colours)



Using G_c^* from experiment, the number of cycles to failure (N_f) were calculated in simulation as

$$G_c^* = \int_1^{ss} \dot{U}^{cp} \zeta dN + \int_{ss}^{N_f} \dot{U}^{cp} \zeta dN \tag{8}$$

where ζ is the fraction of the plastic energy storage and dissipation during deformation. A constant value of 1 for ζ has been assigned in the study. From the first cycle to the cycle of saturated loop (ss), until the cycle of failure (N_f) refer to number of cycles recorded by simulation. The energy per cycle per unit volume associated with plastic deformation in equation (8) is calculated as $\dot{U}^{cp} = \int | \sigma : d\epsilon^p |$ in the CPFE modelling. Here the value for stress and strain is calculated and recorded during simulation. The predicted S-N curve indicates that the fatigue strength of columnar microstructure is relatively higher than the equiaxed microstructure in low cycle fatigue regime.

As the number of fatigue cycles increased above the 103 cycles, the equiaxed microstructure shows better performance. This is consistent with the effect of strain accumulation in the columnar microstructure. As discussed above, when the stress reaches to critical crack nucleation energy, the crack initiates and with further increase in cycle, it will grow and eventually fracture occurs. In columnar grains, due to the stress concentration effect, the critical value reaches at lower number of cycles. But in case of equiaxed microstructure when the stress is higher, it relaxed by operating the other deformation mechanism leading to an effective stress-relaxation. These phenomena lead to delay the crack initiations at the sample number of applied cycles, thereby increase the fatigue life. This is consistent with the literature data, where it has been indicated that the equiaxed microstructure shown better fatigue performance compare to the columnar structure.

4 Conclusions

The deformation behaviour of IN 718 is studied considering the two extreme microstructural characteristics typically observed in fusion-based AM techniques such as columnar and equiaxed microstructure using CP modelling that are. It is demonstrated that the behaviour of two microstructures in the absence of defects such as porosity or residual stress can on the fatigue response changes with the number of cycles. The GBs of the columnar structure essentially acts as stress concentration sites for the deformation. The strain concentration effect of these GBs is largely affected by their orientation with respect to the cyclic loading direction. The columnar microstructure indicates comparatively high cyclic hardening to the equiaxed microstructure with increased strain amplitudes. It is observed that at the low number of cycles, the columnar microstructure shown better fatigue performance. This is attributed to the hardening effect due to the stress concentration effect by the GBs. At the higher number of cycles (>103), the equiaxed microstructure shown relatively better performance. The enhanced fatigue performance was due to the delay in crack initiation due to the stress relaxation effect. This study offers a design consideration to improve the fatigue performance of the AM IN 718.

Acknowledgements

LTM thank the College of Engineering, University of Nevada Reno for funding. PK sincerely acknowledges the funding from the University of New Mexico. Authors thank reviewers for the constructive comments during the review process.

References

- Armstrong, P.J. and Frederick, C.O. (1966) *A Mathematical Representation of the Multiaxial Bauschinger Effect*, Central Electricity Generating Board and Berkeley Nuclear Laboratories.
- Aydinöz, M.E., Brenne, F., Schaper, M., Schaak, C., Tillmann, W., Nellesen, J. and Niendorf, T. (2016) ‘On the microstructural and mechanical properties of post-treated additively manufactured Inconel 718 superalloy under quasi-static and cyclic loading’, *Mater. Sci. Eng. A*, Vol. 669, pp.246–258 [online] <https://doi.org/10.1016/j.msea.2016.05.089>.
- Babamiri, B.B., Indeck, J., Demeneghi, G., Cuadra, J. and Hazeli, K. (2020) ‘Quantification of porosity and microstructure and their effect on quasi-static and dynamic behavior of additively manufactured Inconel 718’, *Addit. Manuf.*, Vol. 34, p.101380 [online] <https://doi.org/10.1016/j.addma.2020.101380>.
- Bajaj, P., Hariharan, A., Kini, A., Kürnsteiner, P., Raabe, D. and Jägle, E.A. (2020) ‘Steels in additive manufacturing: a review of their microstructure and properties’, *Mater. Sci. Eng. A*, Vol. 772, p.138633 [online] <https://doi.org/10.1016/j.msea.2019.138633>.
- Balachandramurthi, A.R., Moverare, J., Dixit, N. and Pederson, R. (2018) ‘Influence of defects and as-built surface roughness on fatigue properties of additively manufactured Alloy 718’, *Mater. Sci. Eng. A*, Vol. 735, pp.463–474 [online] <https://doi.org/10.1016/j.msea.2018.08.072>.
- Biffi, C.A., Fiochi, J., Ferrario, E., Fornaci, A., Riccio, M., Romeo, M. and Tuissi, A. (2020) ‘Effects of the scanning strategy on the microstructure and mechanical properties of a Ti-6Al-4V alloy produced by electron beam additive manufacturing’, *Int. J. Adv. Manuf. Technol.*, Vol. 107, pp.4913–4924 [online] <https://doi.org/10.1007/s00170-020-05358-y>.

- Cao, F. and Ravi Chandran, K.S. (2016) 'Fatigue performance of powder metallurgy (PM) Ti-6Al-4V alloy: a critical analysis of current fatigue data and metallurgical approaches for improving fatigue strength', *JOM*, Vol. 68, pp.735–746 [online] <https://doi.org/10.1007/s11837-016-1821-5>.
- Cao, F., Kumar, P., Koopman, M., Lin, C., Fang, Z.Z. and Chandran, K.S.R. (2015) 'Understanding competing fatigue mechanisms in powder metallurgy Ti-6Al-4V alloy: role of crack initiation and duality of fatigue response', *Mater. Sci. Eng. A*, Vol. 630, pp.139–145 [online] <https://doi.org/10.1016/j.msea.2015.02.028>.
- Cruzado, A., Llorca, J. and Segurado, J. (2017) 'Modeling cyclic deformation of Inconel 718 superalloy by means of crystal plasticity and computational homogenization', *Int. J. Solids Struct.*, Vols. 122–123, pp.148–161 [online] <https://doi.org/10.1016/j.ijsolstr.2017.06.014>.
- Dehoff, R.R., Kirka, M.M., Sames, W.J., Bilheux, H., Tremsin, A.S., Lowe, L.E. and Babu, S.S. (2015) 'Site specific control of crystallographic grain orientation through electron beam additive manufacturing', *Mater. Sci. Technol.*, Vol. 31, pp.931–938 [online] <https://doi.org/10.1179/1743284714Y.0000000734>.
- Deng, W., Xu, J., Hu, Y., Huang, Z. and Jiang, L. (2019) 'Isothermal and thermomechanical fatigue behavior of Inconel 718 superalloy', *Mater. Sci. Eng. A*, Vol. 742, pp.813–819 [online] <https://doi.org/10.1016/j.msea.2018.11.052>.
- Frazier, W.E. (2014) 'Metal additive manufacturing: a review', *J. Mater. Eng. Perform.*, Vol. 23 [online] <https://doi.org/10.1007/s11665-014-0958-z>.
- Holland, S., Wang, X., Fang, X., Guo, Y., Yan, F. and Li, L. (2018) 'Grain boundary network evolution in Inconel 718 from selective laser melting to heat treatment', *Mater. Sci. Eng. A*, Vol. 725, pp.406–418.
- Jackson, P.J. and Basinski, Z.S. (2011) 'Latent hardening and the flow stress in copper single crystals', *Can. J. Phys.* [online] <https://doi.org/10.1139/p67-055>.
- Kocks, U.F. and Brown, T.J. (1966) 'Latent hardening in aluminum', *Acta Metall.*, Vol. 14, pp.87–98 [online] [https://doi.org/10.1016/0001-6160\(66\)90290-2](https://doi.org/10.1016/0001-6160(66)90290-2).
- Kumar, P. and Chandran, K.S.R. (2017) 'Strength-ductility property maps of powder metallurgy (PM) Ti-6Al-4V alloy: a critical review of processing-structure-property relationships', *Metall. Mater. Trans. A*, Vol. 48, pp.2301–2319 [online] <https://doi.org/10.1007/s11661-017-4009-x>.
- Kumar, P., Farah, J., Akram, J., Teng, C., Ginn, J. and Misra, M. (2019) 'Influence of laser processing parameters on porosity in Inconel 718 during additive manufacturing', *Int. J. Adv. Manuf. Technol.*, Vol. 103, pp.1497–1507 [online] <https://doi.org/10.1007/s00170-019-03655-9>.
- Lee, E.H. (1969) 'Elastic-plastic deformation at finite strains', *J. Appl. Mech.*, Vol. 36, pp.1–6.
- Lewandowski, J.J. and Seifi, M. (2016) 'Metal additive manufacturing: a review of mechanical properties', *Annu. Rev. Mater. Res.*, Vol. 46, pp.151–186 [online] <https://doi.org/10.1146/annurev-matsci-070115-032024>.
- Li, X., Shi, J.J., Cao, G.H., Russell, A.M., Zhou, Z.J., Li, C.P. and Chen, G.F. (2019) 'Improved plasticity of Inconel 718 superalloy fabricated by selective laser melting through a novel heat treatment process', *Mater. Des.*, Vol. 180, p.107915 [online] <https://doi.org/10.1016/j.matdes.2019.107915>.
- McGinty, R.D. (2002) 'Multiscale representation of polycrystalline inelasticity'.
- NASA (2017) *Specification for Central and Qualification of Laser Powder Bed Fusion Metallurgical Processes*, Marshall Space Flight Center, Alabama.
- Ni, M., Liu, S., Chen, C., Li, R., Zhang, X. and Zhou, K. (2019) 'Effect of heat treatment on the microstructural evolution of a precipitation-hardened superalloy produced by selective laser melting', *Mater. Sci. Eng. A*, Vol. 748, pp.275–285.

- Shi, R., Khairallah, S.A., Roehling, T.T., Heo, T.W., McKeown, J.T. and Matthews, M.J. (2020) 'Microstructural control in metal laser powder bed fusion additive manufacturing using laser beam shaping strategy', *Acta Mater.*, Vol. 184, pp.284–305 [online] <https://doi.org/10.1016/j.actamat.2019.11.053>.
- Vikram, R.J., Singh, A. and Suwas, S. (2020) 'Effect of heat treatment on the modification of microstructure of selective laser melted (SLM) IN 718 and its consequences on mechanical behavior', *J. Mater. Res.*, Vol. 35, pp.1949–1962 [online] <https://doi.org/10.1557/jmr.2020.129>.
- Wu, Y., Bönisch, M., Alkan, S., Abuzaid, W. and Sehitoglu, H. (2018) 'Experimental determination of latent hardening coefficients in FeMnNiCoCr', *Int. J. Plast.* Vol. 105, pp.239–260 [online] <https://doi.org/10.1016/j.ijplas.2018.02.016>.
- Ye, W., Akram, J. and Mushongera, L.T. (2020) 'Fatigue behavior of additively manufactured IN 718 with columnar grains', *Adv. Eng. Mater.* [online] <https://doi.org/10.1002/adem.202001031>.
- Zhao, Z. and Chen, X. (2020) 'Effect of cyclic softening and stress relaxation on fatigue behavior of 2.25Cr1Mo0.25V steel under strain-controlled fatigue-creep interaction at 728 K', *Int. J. Fatigue*, Vol. 140, p.105848 [online] <https://doi.org/10.1016/j.ijfatigue.2020.105848>.
- Zhou, Z., Hua, X., Li, C. and Chen, G. (2018) 'The effect of texture on the low cycle fatigue property of Inconel 718 by selective laser melting', *MATEC Web Conf.*, Vol. 165, p.2007 [online] <https://doi.org/10.1051/mateconf/201816502007>.